

# Atomic Structure Control of Size-Selected Gold Nanoclusters during Formation

Simon R. Plant, Lu Cao, and Richard E. Palmer\*

Nanoscale Physics Research Laboratory, School of Physics and Astronomy, University of Birmingham, Birmingham B15 2TT, United Kingdom

**ABSTRACT:** We report the ability to control the atomic structure of nanoclusters by systematically varying the gas-phase formation parameters during the generation of size-selected Au<sub>923</sub>. From aberration-corrected, scanning transmission electron microscopy (HAADF-STEM) imaging, we are able to identify the proportions of icosahedral (Ih), decahedral (Dh), and face-centered cubic (fcc) isomers within a set of populations, with each population corresponding to a specific set of formation conditions. We demonstrate that, by tuning the formation conditions, we can eliminate completely all icosahedral nanoclusters, which are commonly found under other conditions. In future, this approach may lead to the preparation of arrays or ensembles of nanoclusters containing a dominant or single isomer, thus enabling the investigation of nanocluster (or nanoparticle) properties as a function of both size and atomic configuration.

Controlling the structure of materials at the nanoscale remains a considerable challenge, not least if control is to extend down to the atomic level. The properties of nanoparticles are strongly dependent on size, structure, and composition, and for this reason, the modeling of nanoparticle (or nanocluster) morphology has gained considerable attention in recent years,<sup>1,2</sup> especially for gold.<sup>3,4</sup> Gold nanoparticles or nanoclusters are used extensively in many applied research areas, particularly for catalysis,<sup>5–7</sup> in plasmonics<sup>8</sup> and for the growth of nanomaterials such as Si nanowires.<sup>9</sup> Cluster ion beam deposition combined with mass selection permits the highly controlled generation of nanoclusters in terms of particle size, deposition energy, and coverage (average density) on a substrate surface.<sup>10,11</sup> The technique currently allows the preparation of supported nanoclusters to investigate their size-dependent properties, an example being catalysis under realistic reaction conditions.<sup>12</sup> Even for a specific size, however, nanoclusters can exhibit a range of atomic configurations, as demonstrated for size-selected Au<sub>20</sub>,<sup>13</sup> Au<sub>55</sub>,<sup>14</sup> Au<sub>309</sub>,<sup>15</sup> and Au<sub>923</sub>,<sup>16,17</sup> many of which differ significantly from the bulk. Given the importance of atomic configuration in determining the active sites of catalytic nanoparticles,<sup>18</sup> the ability to control isomer populations during formation would be greatly advantageous, in general enabling the properties of nanoclusters to be correlated with their atomic structures. Varying the formation conditions in the cluster beam source has thus far been used to influence core–shell composition for bimetallic Au–Cu nanoclusters.<sup>19</sup>

Here, we report the ability to tune the atomic structure of size-selected nanoclusters at the formation stage by varying the gas-phase cluster formation parameters when generating Au<sub>923</sub>, such that we can eliminate all icosahedra (Ih). Ih-Au<sub>923</sub> has previously been identified as a metastable structure by monitoring beam-induced structural transformations in the electron microscope.<sup>16</sup> We determine the statistical proportions of isomers within each sample population of Au<sub>923</sub> nanoclusters by comparing the structure as observed in HAADF-STEM (high-angle annular dark field-scanning transmission electron microscopy) imaging with multislice image simulations from the current simulation atlas of Au<sub>923</sub>.<sup>20</sup> We demonstrate that the proportion of icosahedral nanoclusters within the population varies monotonically as a function of both magnetron power and condensation length over the parameter space under investigation. These results open the way to investigating nanocluster properties as a function of both size and atomic configuration.

Size-selected Au<sub>923</sub> nanoclusters were produced using a magnetron-sputtering gas-condensation cluster beam source<sup>21,22</sup> coupled to an inline, lateral time-of-flight mass selector<sup>23</sup> with a nominal mass resolution of  $M/\Delta M \approx 20$ . The mass resolution employed yields nanoclusters containing  $923 \pm 23$  atoms. Parameters including magnetron power (DC), condensation length, gas pressure, and gas flow were varied during synthesis. The nanoclusters were soft-landed (1.5 keV per nanocluster) directly onto amorphous carbon films in high vacuum in order to preserve, insofar as possible, the free space structure. Atomic resolution imaging was performed using a JEOL JEM 2100F STEM operating at 200 keV and equipped with a spherical aberration probe corrector (CEOS GmbH) and a HAADF detector with an inner collection angle of 62 mrad. In total, more than 1200 clusters were analyzed to provide the statistical proportions of isomers within the various populations.

Figure 1a–c shows structural models of high symmetry isomers for Au<sub>923</sub>. Figure 1d–g presents example HAADF-STEM images of Au<sub>923</sub> nanoclusters characteristic of the icosahedral (Ih) and decahedral (Dh) isomers, both of which exhibit 5-fold symmetry axes, and also the face-centered cubic (fcc) isomer. As observed previously,<sup>16</sup> the Dh-Au<sub>923</sub> nanoclusters may be found to exhibit, in part, the re-entrant structure characteristic of the Marks truncated decahedron (Figure 1g), in spite of the fact that Au<sub>923</sub> is not a “magic number” for the Marks decahedron. The Ih-Au<sub>923</sub> nanoclusters are readily identified owing to the unique geometric patterns of

Received: March 18, 2014

Published: May 6, 2014

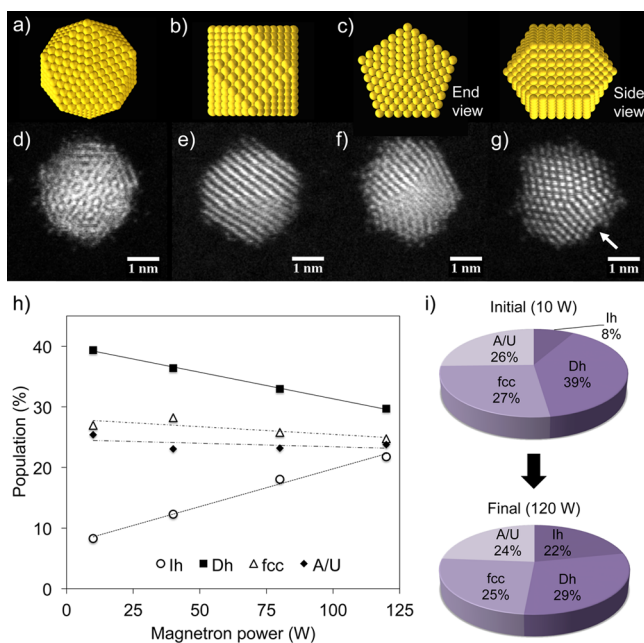


**Figure 1.** (a–c) Models of the icosahedral (a), face-centered cubic (cuboctahedron shown in (b)) and Ino-decahedral (c) isomers of  $\text{Au}_{923}$ . (d–g) Typical HAADF-STEM images of the following  $\text{Au}_{923}$  nanocluster isomers: (d) an icosahedron (Ih) viewed close to a 5-fold symmetry axis, (e) face-centered cubic (fcc) polyhedron, (f) a decahedron (Dh) viewed off-axis, and (g) a decahedron clearly exhibiting a partial Marks-type reconstruction (example of a re-entrance marked with a white arrow) viewed along its 5-fold symmetry axis. (h) A plot of the relative abundances for fcc, Dh, and Ih isomers within a given population of  $\text{Au}_{923}$  nanoclusters as a function of the magnetron power used during their formation. A/U represents the proportion of amorphous or unassigned structures. (i) The compositions of the initial and final populations over the whole parameter space. Related parameters: condensation length, 250 mm; Ar gas flow, 200 sccm; He gas flow, 180 sccm; pressure, 0.43 mbar; deposition energy, 1500 eV.

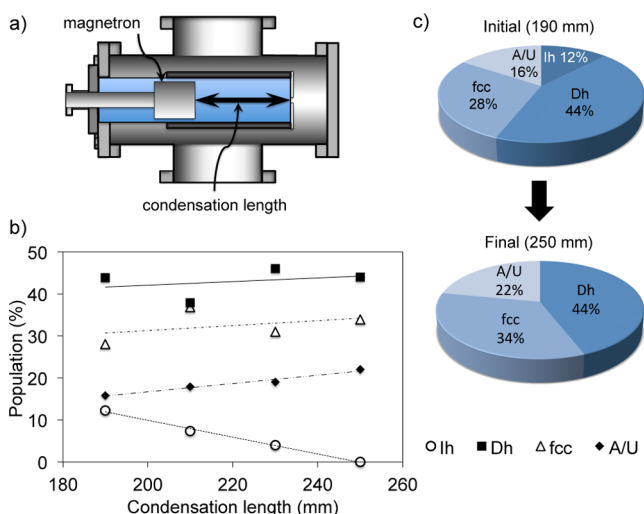
their structural motifs in the HAADF-STEM images. In any given population, we find that there are a number of nanoclusters that cannot be assigned uniquely to either fcc or Dh structures, and there are nanoclusters that cannot be assigned to an ordered structure at all, due to their amorphous appearance. We do not arbitrarily exclude such nanoclusters from the data set, and we therefore designate the structure of each nanocluster as belonging to one of four categories: Ih, Dh, fcc, and, finally, amorphous or unassigned (A/U).

Figure 1h shows a plot of the relative abundances of isomers observed within a given population as a function of magnetron power over the range 10–120 W. Figure 1i highlights the initial and final states of the populations over the full range. Note that the deposition energy of 1.5 keV per cluster equates to 1.6 eV/atom, which lies far below the typical pinning threshold for Au clusters on carbon (graphite).<sup>24,25</sup> Previous studies of soft-landed, size-selected  $\text{Au}_{923}$  nanoclusters have used deposition energies of 0.5 eV/atom on amorphous carbon films and 5.4 eV/atom on few-layer graphene films, respectively.<sup>16,17</sup> Figure 1h shows that the Dh- $\text{Au}_{923}$  isomer is found always to be the most abundant, with no significant variation in the proportions of  $\text{Au}_{923}$  nanoclusters exhibiting fcc or unidentified/amorphous structures over this parameter space. These results compare favorably with the predictions of Li et al.<sup>15</sup> which state that, although below 100 atoms the Ih isomer is more stable than

either the Dh or cuboctahedron, at larger sizes of up to 1000 atoms, Ino-Dh is most favored. Koga et al.<sup>26</sup> have shown experimentally that, although the vast majority of Au nanoparticles near 3 nm in size (and therefore comparable to  $\text{Au}_{923}$ ) are icosahedral when produced in the gas phase by rapid cooling of atomic vapor, many later convert to Dh through thermal annealing. Indeed, the Ih-to-Dh structural transition was the more frequent transformation for  $\text{Au}_{923}$  nanoclusters observed in the electron microscope.<sup>16</sup> Therefore, it is likely that the Dh isomer represents an equilibrium structure at this size. The interplay between Dh- $\text{Au}_{923}$  and Ih- $\text{Au}_{923}$  is also reflected in the present results, given that the proportion of Dh- $\text{Au}_{923}$  declines monotonically (gradient  $-0.09$ ,  $R^2 > 0.99$ ) as a function of increasing magnetron power, while the proportion of Ih- $\text{Au}_{923}$  rises (gradient  $0.12$ ,  $R^2 = 0.99$ ). We wish to emphasize the role of reaction kinetics here: we vary only the magnetron power, the parameter that controls the sputtering rate of the bulk gold target used to produce the supersaturated atomic vapor from which the clusters form.

This leads us to consider the microscopic growth mechanism for the nanoclusters, as the results imply that the Ih isomer is favored under formation conditions where the supersaturated atomic vapor is most dense. The observation of ordered, metastable icosahedra may be attributable to a *kinetic trapping effect*,<sup>1</sup> whereby larger icosahedra form from smaller, icosahedral “seeds” through the addition of successive and complete geometric shells.<sup>26,27</sup> This is supported by molecular dynamics simulations indicating that ideal atom-wise growth produces icosahedra almost exclusively, whereas coalescence gives rise to Dh and fcc structures.<sup>28</sup> Increasing the magnetron power, and therefore the sputtering rate, results in a higher density of Au atoms available in the supersaturated atomic vapor, favoring more rapid growth and driving growth conditions further from equilibrium. It is notable that there is little variation in the proportion of fcc- $\text{Au}_{923}$  nanoclusters observed across this parameter space, and it may be the case that the formation of the fcc structure is therefore dominated by thermodynamic effects.

We now consider the effect of the condensation length, defined by the cluster source geometry, on the relative abundance of isomers within a given population. A detailed explanation of the configuration of the cluster source apparatus is provided in ref 22; however, it is worth stating that the cluster generation chamber houses an internal condensation chamber cooled with liquid  $\text{N}_2$  (Figure 2a). Cluster ions are extracted from the condensation chamber, exiting through an adjustable aperture (iris), which is used to control pressure within the condensation chamber independently of the gas flows. The condensation length is thus defined by the distance from the head of the magnetron (i.e., the source of atomic vapor) to the end of the condensation chamber, where the adjustable aperture is located. The condensation length can be varied by adjusting the position of the magnetron head within the chamber. Figure 2b shows a plot of the relative abundances of fcc, Dh, and Ih isomers observed within a given population as a function of condensation length (in the range of 190–250 mm). The magnetron power was fixed at 10 W, and all other parameters were the same as those used for the investigation of the magnetron power pertaining to Figure 1, except for a difference of 0.04 mbar in the pressure recorded in the condensation chamber. We suggest that this may account for shifts in the proportions of fcc, Dh, and Ih isomers between the two data sets shown in Figures 1 and 2, even where all other



**Figure 2.** (a) Schematic diagram showing the internal condensation chamber housed within the generation chamber of the cluster source apparatus. The condensation length, as defined by the distance between the magnetron head and the exit aperture, is denoted by the double-headed arrow. (b) A plot of the relative abundances of face-centered cubic (fcc), decahedral (Dh), and icosahedral (Ih) isomers within a given population of  $\text{Au}_{923}$  nanoclusters as a function of the condensation length used during their formation. A/U represents the proportion of amorphous or unassigned clusters. (c) The compositions of the initial and final populations over the whole parameter space. Related parameters: magnetron power, 10 W (DC); Ar gas flow, 200 sccm; He gas flow, 180 sccm; pressure, 0.39 mbar; deposition energy, 1500 eV.

parameters were identical (magnetron power, 10 W; condensation length, 250 mm). We do observe the same overall trend in this case, however, whereby the Dh isomer is most abundant (near 40%) and the Ih isomer least (<10%). Figure 2c emphasizes the transformation between the initial and final compositions of the populations over the full parameter space.

Figure 2b indicates that there is a competition between the fcc and Dh isomers with increasing condensation length, although the overall trend is for proportions of both isomers to increase. It is evident, however, that there is a decline (gradient  $-0.20$ ,  $R^2 = 0.99$ ) in the proportion of Ih- $\text{Au}_{923}$  nanoclusters as a function of increasing condensation length, such that at the longest condensation length (for which the cluster source geometry allows) the icosahedra are brought to extinction. This represents the largest condensation volume, as the volume bounded by the condensation chamber walls and the head of the magnetron varies in direct proportion with the condensation length,  $L$ . For constant magnetron power (and therefore sputtering rate), the average concentration of the atomic vapor in the volume defined by the condensation length varies as  $1/L$ , resulting in an increase in the mean free path of the atomic clusters, and permitting slower growth times prior to the nanoclusters emerging from the aperture at the end of the condensation chamber. Hence, the reaction kinetics move more toward equilibrium with increasing condensation length, such that the *kinetic trapping effect* is reduced, and whereby we observe higher proportions of the (equilibrium) Dh isomer, as well as bulk-like fcc.

In summary, we have used HAADF-STEM imaging combined with multislice image simulations to identify the statistical proportions of isomers within populations of  $\text{Au}_{923}$  nanoclusters as a function of the parameters used during their

formation. We have thereby demonstrated that the atomic structure of size-selected nanoclusters deposited from the gas phase can be tuned by varying the formation parameters. Significantly, we show that, over the parameter space under investigation, there is a monotonic relationship between the proportion of icosahedral isomers and both magnetron power and condensation length, such that we are able to eliminate all Ih isomers for a specific set of formation parameters. Under nonequilibrium conditions, we reveal the interplay between the isomers exhibiting 5-fold symmetry axes, whereby the proportion of Dh is sacrificed in favor of Ih. The approach presented here may allow the preparation of arrays or ensembles which are isomerically pure, thus enabling the investigation of nanocluster (or nanoparticle) properties, as a function not only of size, but also atomic configuration.

## AUTHOR INFORMATION

### Corresponding Author

r.e.palmer@bham.ac.uk

### Notes

The authors declare no competing financial interest.

## ACKNOWLEDGMENTS

This work was funded by EPSRC and by the Science City AM2 (Advanced Materials) project. S.R.P. acknowledges support through a Science City Research Alliance Fellowship, which is funded by the Higher Education Funding Council for England (HEFCE). L.C. acknowledges doctoral funding provided by the China Scholarship Council (CSC) and the School of Physics and Astronomy, University of Birmingham.

## REFERENCES

- Baletto, F.; Ferrando, R. *Rev. Mod. Phys.* **2005**, *77*, 371.
- Barnard, A. S. *Rep. Prog. Phys.* **2010**, *73*, 086502.
- Barnard, A. S.; Young, N. P.; Kirkland, A. I.; van Huis, M. A.; Xu, H. *ACS Nano* **2009**, *3*, 1431.
- Barnard, A. S. *Acc. Chem. Res.* **2012**, *45*, 1688.
- Sanchez, A.; Abbet, S.; Heiz, U.; Schneider, W.-D.; Häkkinen, H.; Barnett, R. N.; Landman, U. *J. Phys. Chem. A* **1999**, *103*, 9573.
- Boyen, H.-G.; Kästle, G.; Weigl, F.; Koslowski, B.; Dietrich, C.; Ziemann, P.; Spatz, J. P.; Riethmüller, S.; Hartmann, C.; Möller, M.; Schmid, G.; Garnier, M. G.; Oelhafen, P. *Science* **2002**, *297*, 1533.
- Harding, C.; Habibpour, V.; Kunz, S.; Farnbacher, A. N.-S.; Heiz, U.; Yoon, B.; Landman, U. *J. Am. Chem. Soc.* **2009**, *131*, 538.
- Maier, S. A.; Brongersma, M. L.; Kik, P. G.; Meltzer, S.; Requicha, A. A. G.; Atwater, H. A. *Adv. Mater.* **2001**, *13*, 1501.
- Wu, Y.; Cui, Y.; Huynh, L.; Barrelet, C. J.; Bell, D. C.; Lieber, C. M. *Nano Lett.* **2004**, *4*, 433.
- Bromann, K.; Félix, C.; Brune, H.; Harbich, W.; Monot, R.; Buttet, J.; Kern, K. *Science* **1996**, *274*, 956.
- Palmer, R. E.; Pratontep, S.; Boyen, H.-G. *Nat. Mater.* **2003**, *2*, 443.
- Habibpour, V.; Song, M. Y.; Wang, Z. W.; Cookson, J.; Brown, C. M.; Bishop, P. T.; Palmer, R. E. *J. Phys. Chem. C* **2012**, *116*, 26295.
- Wang, Z. W.; Palmer, R. E. *Nanoscale* **2012**, *4*, 4947.
- Wang, Z. W.; Palmer, R. E. *Nano Lett.* **2012**, *12*, 5510.
- Li, Z. Y.; Young, N. P.; Di Vece, M.; Palomba, S.; Palmer, R. E.; Bleloch, A. L.; Curley, B. C.; Johnston, R. L.; Jiang, J.; Yuan, J. *Nature* **2008**, *451*, 46.
- Wang, Z. W.; Palmer, R. E. *Phys. Rev. Lett.* **2012**, *108*, 245502.
- Plant, S. R.; Cao, L.; Yin, F.; Wang, Z. W.; Palmer, R. E. *Nanoscale* **2014**, *6*, 1258.
- Falsig, H.; Hvorbæk, B.; Kristensen, I. S.; Jiang, T.; Bligaard, T.; Christensen, C. H.; Nørskov, J. K. *Angew. Chem.* **2008**, *120*, 4913.

(19) Yin, F.; Wang, Z. W.; Palmer, R. E. *J. Am. Chem. Soc.* **2011**, *133*, 10325.

(20) Supporting Information to ref 16.

(21) Goldby, I. M.; von Issendorff, B.; Kuipers, L.; Palmer, R. E. *Rev. Sci. Instrum.* **1997**, *68*, 3327.

(22) Pratontep, S.; Carroll, S. J.; Xirouchaki, C.; Streun, M.; Palmer, R. E. *Rev. Sci. Instrum.* **2005**, *76*, 045103.

(23) von Issendorff, B.; Palmer, R. E. *Rev. Sci. Instrum.* **1999**, *70*, 4497.

(24) Di Vece, M.; Palomba, S.; Palmer, R. E. *Phys. Rev. B* **2005**, *72*, 073407.

(25) Smith, R.; Nock, C.; Kenny, S. D.; Belbruno, J. J.; Di Vece, M.; Palomba, S.; Palmer, R. E. *Phys. Rev. B* **2006**, *73*, 125429.

(26) Koga, K.; Ikeshoji, T.; Sugawara, K. *Phys. Rev. Lett.* **2004**, *92*, 115507.

(27) Baletto, F.; Mottet, C.; Ferrando, R. *Phys. Rev. B* **2001**, *63*, 155408.

(28) Grochola, G.; Russo, S. P.; Snook, I. K. *J. Chem. Phys.* **2007**, *126*, 164707.

#### ■ NOTE ADDED AFTER ASAP PUBLICATION

This paper was published ASAP on May 14, 2014 with incorrect figures. Figure 1 was corrected and Figures 1 and 2 were returned to the proper sequence. The corrected version was reposted on May 15, 2014.